Geochemical Perspectives Letters

Halogens in proto-Iceland plume basalts

E.L. Tomlinson, E.F. Rose-Koga, A-S Bouvier, D. O'Farrell, J.T. Caulfield, M.G. Jackson, Y. Moussallam, F.M. Stuart, J. Villeneuve

Supplementary Information

The Supplementary Information includes:

- Methods
- Major Element Compositions
- Halogen Partitioning Calculation
- Tables S-1 to S-6
- Figure S-1 to S-4
- Supplementary Information References

Methods

Sample preparation

Olivine crystals from the selected PIP lava flows are medium sized (300-500 µm) equant and tabular crystals. Olivine grains containing melt inclusions were hand-picked under transmitted light at 50-100× magnification, care was taken to avoid inclusions that were open or connected to cracks or spinel mineral inclusions. Melt inclusions are rounded, optically clear to pink glasses, ranging in size from 20 to 100 µm (Fig. S-1). Where possible, we selected clean, glassy inclusions. Melt inclusions in sample 332901 were re-homogenised using a Vernadsky-type microscope heating stage at 1-atm (Sobolev *et al.*, 1980; Schiano, 2003) following the procedure described in Le Voyer *et al.* (2010). In short, a partially crystallized melt inclusion is put in a 1-atm oven in which the oxygen fugacity is kept low at 10^{-10} atm with purified He with Zr at 700 ºC to avoid oxidation of the host crystal and to facilitate a rapid quench. We increased the temperature at a rate of about 8ºC/min and visually monitored the regular disappearance of crystals in the melt inclusion. Once all crystals had melted inside the melt inclusion, we kept the temperature constant for 5 more minutes and then quenched the experiment. The heating procedure was completed in less than 30 minutes. Selected olivine grains were mounted onto individual glass slides using Crystalbond 509 and then individually polished by hand using progressively fining grit SiC papers and then diamond paste to expose the melt inclusions. The melt inclusion-bearing olivines were liberated from the Crystalbond and mounted in a Struers Epofix resin mount before receiving a final ¼ µm diamond paste polish on an automated polisher. The mount was then analysed for major elements and chlorine isotopes. The melt inclusion-bearing olivine grains were then liberated from the epoxy mount and cleaned in acetone and distilled water before being pressed into indium (Rose-Koga *et al.*, 2021) for elemental halogen analysis by SIMS.

Major element analysis (EMPA-WDS and SEM-EDX)

Major element compositions of PIP melt inclusions were analysed using a JEOL 8600 electron microprobe equipped with 4 wavelength dispersive spectrometers (EMPA-WDS) at the Research Laboratory for Archaeology and the History of Art (RLAHA), University of Oxford. Data were acquired at an accelerating voltage of 15 KeV, a beam current of 5 nA and a beam diameter of 5 µm. Peak count times were 30-70 s on each peak except for Na (12 s). The instrument was calibrated for the beam conditions using a suite of appropriate mineral standards and count rates were corrected using the PAP absorption correction method. Volatile elements were also analysed by EMPA-WDS at the RLAHA. Analyses used peak counting times of 120 s for F, P and S and 30 s for Cl, however both F and Cl were below the detection limits of 0.11 and 0.03 %, respectively. A summary of the analytical conditions for each element is given below.

	Crystal	Peak count time (s)	Background count time either side of peak (s)
Na	TAP	12	6
Mg	TAP	70	35
Al	TAP	50	25
Si	TAP	30	15
K	PET	30	15
Ca	PET	30	15
Ti	PET	30	15
Mn	LIF	40	20
Fe	LIF	40	20
F	LDE	120	60
P	TAP	120	60
Cl	PET	30	15
Cr	PET	60	30
S	PET	120	120

Additional major element analyses were undertaken at the iCRAG laboratory at Trinity College Dublin using a using a Tescan Mira XMU field-gun emission scanning electron microscope equipped with an XMAX 80 nm^2 energy dispersive (SEM-EDS) detector. Measurements were conducted using an accelerating voltage of 20 kV and a beam current of 300 pA. A suite of appropriate mineral standards from the Smithsonian Institute (Jarosewich *et al.*, 1980) was used to calibrate the instrument for quantitative analyses. Totals acquired were all within ±1 % of 100 wt. %. Both EMPA-WDS and SEM-EDS methods were verified using the StHs6/80-G and GOR128-G MPI-DING reference glasses from the Max Planck Institute (Jochum *et al.*, 2006) and accuracy (%bias) and precision (%RSD) are typically better than ± 5 % for both methods for all elements at concentrations above 0.5 wt. %. Data is provided in Table S-1.

Elemental halogen analysis

Halogen concentrations of PIP melt inclusions were analysed by secondary ion mass spectrometry (SIMS) using a CAMECA ims1280-HR at Centre de Recherches Pétrographiques et Géochimiques. The samples were sputtered with a Cs^+ primary beam at an accelerating voltage of 10 kV and focused as a 15 µm beam size on the sample. Each spot was sputtered either for 300 sec with a 6µm rastered beam of 0.5 nA in 2022 or for 60 sec with a 5µm rastered beam of a stronger primary intensity of 3nA in 2019. The electron gun was used for charge compensation at the surface of the sample. Negative secondary ions were extracted through a potential of 10 kV and measured in peak jumping mode on several EM detectors. Analytical conditions are shown below.

Date	10-11 April 2019 Br	12 April 2019 Volatile elements	11-12 July 2022 Halogens
Masses	76.85 (background) $^{29}Si^{16}O_3$, $^{30}Si^{16}O_3$, ^{79}Br, ^{81}Br	11.8 (background FC), 11.9 (background EM) ^{12}C, ^{17}O, $^{16}O^1H$, ^{18}O, ^{19}F, ^{27}Al, ^{30}Si, ^{32}S, ^{35}Cl,	17.8O (background) ^{18}O, ^{19}F, ^{27}Al, ^{30}Si, ^{35}Cl, ^{79}Br, ^{81}Br,
Energy filtering	20 eV	20 eV	30 eV
Primary beam current	3.4 nA	1 nA	0.5 nA
Pre sputter	60 s	60 s	300 s
Raster area	5 x 5 µm	10 x 10 µm	6 x 6 µm
MRP	21000	7500	22000
Analysis time	4 s (background) 4 s, 4 s, 12 s, 12 s	2 s, 1 s (background) 4s, 2s, 4s, 4s, 2s, 2s, 4s, 4s, 3s	4 s (background) 3 s, 5 s, 3 s, 3 s, 4 s, 10 s, 10 s
Wait time before	2 s for all	2 s, 1 s (background) 1 s for all	4 s (background) 1 s, 1 s, 1 s, 1 s, 1 s, 4 s, 2 s
No. cycles	12	10	10
Approx. analysis time	12 minutes	18 minutes	18 minutes

For analysis of Br, energy filtering was set between +20 to +30 eV to reduce matrix effects. The mass resolving power was set to about 21,000 to separate mass interferences from hydrides (SeH), oxides (CuO) and metals (FeMg, VMg, CrAl and FeAl) on Br. In the 2019 session, Br concentrations were measured in a dedicated Br analysis in which we measured masses 76.85 (background), 77 ($^{29}Si^{16}O_3$), 78 ($^{30}Si^{16}O_3$), 79 (Br) and 81 (Br); these masses were selected to minimize the hysteresis of the magnet. In 2022, we measured Br in the same analysis as F and Cl, so we measured mass ^{79}Br, and ^{81}Br in addition to 17.8 (background), ^{18}O, ^{19}F, ^{27}Al, ^{30}Si, ^{35}Cl and ^{79}Br and ^{81}Br, we used a long wait time of 4s before analysis of ^{79}Br to allow the magnet to settle.

Halogen analyses were calibrated using a suite of natural basalt glasses: VG-2, also known as USNM 111240/52 (Straub and Layne, 2003; Rose-Koga *et al*., 2020) and Macquarie basalt glasses 25603, 40428, 47963 and 60701 (Kendrick *et al.*, 2012; Kendrick *et al*., 2017). The reference values for these glasses and the measured raw counts are summarised in Table S-2 and the resulting calibration curves are shown in figure S-2. We measured both ^{79}Br and ^{81}Br (Fig. S-3), however we use ^{79}Br to quantify Br in the studied samples as this reproduced the known Br contents of the quality control standards more closely. All errors are quoted as 2σ and include both the analytical uncertainty and the propagated error on the calibration curve.

The limit of determination was calculated from the calibration curve using the formula LoD = 3.33 × σ/S, where σ is the standard deviation of the intercept and S is the slope of the calibration curve. Measured reference material compositions are provided in Table S-1. Accuracy is typically better than ±10 %bias for Cl in MPI-DING glasses StHs6/80-G and KL2-G, while the measured concentrations of F in both glasses are slightly low but are within error of the reference values reported by Jochum *et al.* (2006). For Br, accuracy is typically better than ±10 %bias for StHs6/80-G (0.8 ± 0.2 µg.g^{-1}; Jochum *et al.*, 2006), but is worse in KL2-G (0.2 µg.g^{-1}; Jochum *et al.*, 2006) at +30 %bias, suggesting that Br concentration may be overestimated at low abundance. This is particularly true for the 2019 Br data which should be treated with caution as no other Br quality control standard was analysed in this session. Precision for repeat analysis of F, Cl and Br in MPI-DING glass StHs6/80-G is typically better than ±15 %RSD.

Errors on individual halogen analyses are derived from uncertainty on the linear fit of the appropriate calibration curve and errors on halogen ratios for individual melt inclusions are determined by propagating

this calibration uncertainty. For the studied melt inclusions, absolute halogen concentrations may be affected by post entrapment crystallisation (see below), therefore we calculate halogen ratios for individual inclusions where both elements were measured, the average sample values are then the averages of those ratios in melt inclusions from olivines from a given sample lava flow.

Chlorine isotopic analysis

Chlorine isotope compositions were analysed in 2017 using a CAMECA ims1280-HR at the SwissSIMS laboratory, University of Lausanne following a method similar to that of Manzini *et al.* (2017). Samples were sputtered with a 1.5 nA Cs^+ primary beam with an accelerating voltage of 10kV, initially the beam was rastered over an area of 25 µm for 250 s to remove surface Cl contamination. Each analysis consists of 70 cycles of 10 sec, using a rastered beam over an area of 10 µm. It results of a total time per analysis of 17 minutes, included automated centring of the secondary beam in field and contrast apertures. Secondary ions were extracted into the mass spectrometer through a potential of 10 kV, through an energy slit set to a width of 50 eV and were counted on two electron multiplier detectors simultaneously. The mass resolving power was set to ~4800. Glass standards B-21, B-20D (basalts; John *et al.*, 2010) were used for calibration, B-20D was closest to the sample glass composition and so was used to correct for mass fractionation. Additionally, StHs6/80-G and T1-G (andesite and granodiorite; Jochum *et al.*, 2006), for which no bulk $\delta^{37}Cl$ value exists but was proven to give reproducible data, was used to monitor the instrument stability. A drift correction was applied for mount 2 where 4 permil shift was observed for StHs6/80-G. Reproducibility of the StHs6/80-G after drift correction was ~0.4 permil (2 σ). Errors of individual analysis are calculated as two standard errors of the 70 cycles and depends on the Cl content (correlated to count rate) of each melt inclusion compositions.

Major Element Compositions

Host olivines have magnesian cores with forsterite (Fo, Mg/Mg+Fe) of 86-87, most of the studied samples span a fairly narrow compositional range with only weak normal zoning towards their rims (Fo_{83}-Fo_{85}), however olivines from sample 332901 extend to lower forsterite contents (Fo_{76}). The observed forsterite contents are comparable to the composition of olivine expected to be in equilibrium with sample DUR1, a phenocryst-poor lava sample considered to be the most unfractionated of the PIP lavas (Starkey *et al.*, 2012). The olivines have CaO contents of 0.26-0.37 wt. %. High-Mg PIP olivines are considered phenocrysts, rather than xenoliths from the peridotite mantle, because they show smooth continuous trends in Cr_2O_3 and CaO over the range of forsterite, consistent with derivation from the same magmatic system (Larsen and Pedersen, 2000; Starkey *et al.*, 2012). In addition, PIP olivines are characterised by higher CaO for a given forsterite content than olivine from mantle xenoliths from West Greenland (Bernstein *et al.*, 2006), consistent with a high-temperature, low pressure magmatic origin (Jackson and Shirey, 2011).

The melt inclusions have MgO 2.7-8.7 wt. %. This is lower than the whole-rock compositions of their host lavas reported by Starkey *et al.*, (2009), suggesting that they have undergone post entrapment crystallisation (PEC) during which the encapsulated melt crystallises olivine at the inclusion/phenocryst interface during cooling *e.g.* (Sobolev, 1996). Indeed, thin recrystallisation rims are observed in back-scattered electron images of the majority of inclusions. To calculate the liquid line of decent (LLD) of the melt inclusions, equilibrium olivine was subtracted in 0.1 % increments from the whole rock composition of DUR1, a phenocryst poor PIP lava considered to represent the liquid composition (Starkey *et al.*, 2012). The composition of equilibrium olivine was calculated using an equilibrium constant $K_D = 0.3$ (Roedder and Emslie, 1970). Four of the samples, those with glassy melt inclusions, lie on the calculate LLD, suggesting their compositions are consistent with perfect fractional crystallisation of 2-10 % (PI-25, CS-6 and 362077) and 5-25% (CS-5) olivine (Fig. S-4). For samples in which melt inclusions show small degrees of PEC (5-10 %), melt inclusions show a limit range of major element and halogen compositions. The highest K and Cl

contents are found in melt inclusions with the lowest MgO, consistent with evolution on the LLD during PEC of olivine.

Sample 332901 lies off the LLD and has melt compositions suggesting diffusive equilibration between the trapped melt and the host olivine, melt inclusions in this sample were originally crystalised and were homogenised for this study. We have not corrected for PEC because although the halogens are incompatible element during olivine crystallisation and their concentrations will increase in the melt, their ratios in the melt will be unchanged at F>0.1, which is the minimum degree of melting proposed for the PIP source by Herzberg and O'Hara (2002).

Halogen Partition Calculation

Experimental work demonstrates that F is more compatible than Cl in mantle minerals and that both become less incompatible with increasing temperature (Joachim *et al.*, 2015). We use partition coefficients determined at 1500 °C and 2.3 GPa, conditions appropriate for partial melting in the OIB source mantle (Dasgupta *et al*., 2007). We use D_F^{ol}, D_F^{opx}, D_{Cl}^{ol}, and D_{Cl}^{opx} at 1500 °C from figure 4 of Joachim *et al.* (2015). Following Joachim *et al.* (2015) and based on the lower temperature datasets of Hauri *et al.* (2006); Dalou *et al.* (2012); Dalou *et al.* (2014), we assume that D_F^{cpx}/D_F^{opx} is 1.5 and $D_{Cl}^{cpx}/D_{Cl}^{opx}$ is 5. Following Kendrick *et al.*, (2012) we assume that Br and Cl are similarly incompatible ($D_{Br} = D_{Cl}$) in olivine, orthopyroxene and clinopyroxene. In practice, Br may be less compatible than Cl on account of its larger ionic radius, however even if the partition coefficient of Br is two orders lower than that of Cl, this will only affect the calculated composition of the source below ~F=0.1, lower than the degree of melting for both E and N-type PIP magmas proposed by Herzberg and O'Hara (2002). Table S-5 shows the average modal abundances of olivine, orthopyroxene and clinopyroxene in spinel peridotites (McDonough, 1990), excluding minor garnet/spinel, along with the mineral and resulting bulk F, Br and Cl partition coefficients used for accumulated fractional melting modelling. Table S-6 shows the calculated compositions of the PI-25 and CS-6 source regions compared to estimates for the depleted mantle (DM) and bulk silicate Earth (BSE) and data for intraplate lithospheric xenoliths.

Supplementary Tables

Table S-1 Major element, elemental halogen, chlorine isotope compositions of PIP melting inclusions, along with major element compositions of host olivine and published whole rock trace element and isotope compositions.

Table S-1 is available for download (.xlsx) from the online version of this article at http://doi.org/10.7185/geochemlet.2539.

Table S-2 Raw data and reference values used for calibration of F, Cl and Br. Reference values are from: VG-2, also known as USNM 111240/52 (Straub and Layne, 2003; Rose-Koga *et al*., 2020) and Macquarie basalt glasses 25603, 40428, 47963 and 60701 (Kendrick *et al*., 2012; Kendrick *et al*., 2017). Errors on reference values are 2σ. NA – data not available. The limit of determination calculated for each session is also shown.

	F			Cl			Br				
	$^{19}F/^{30}Si$	Error (σ)	F (µg.g^{-1})	$^{35}Cl/^{30}Si$	Error (σ)	Cl (µg.g^{-1})	$^{81}Br/^{30}Si$	Error	$^{79}Br/^{30}Si$	Error	Br (µg.g^{-1})
12/07/2022											
VG2	1.76E-01	1.09E-02	334 ± 14	2.68E-01	1.65E-02	306 ± 13	4.14E-04	1.98E-05	2.95E-04	1.55E-05	NA
VG2	1.85E-01	2.03E-02	334 ± 14	2.57E-01	1.52E-02	306 ± 13	3.92E-04	2.44E-05	2.86E-04	1.99E-05	NA
VG2	1.86E-01	1.28E-02	334 ± 14	2.54E-01	1.42E-02	306 ± 13	3.59E-04	2.26E-05	2.49E-04	1.72E-05	NA
25603	6.09E-01	2.96E-02	769	7.00E-01	3.94E-02	799 ± 17	7.80E-04	4.89E-05	6.10E-04	3.96E-05	2.64 ± 0.06
25603	7.16E-01	4.25E-02	769	7.19E-01	4.84E-02	799 ± 17	7.95E-04	3.89E-05	5.57E-04	2.93E-05	2.64 ± 0.06
25603	5.62E-01	3.12E-02	769	6.91E-01	4.63E-02	799 ± 17	7.85E-04	4.94E-05	5.67E-04	3.67E-05	2.64 ± 0.06
60701	4.69E-01	4.13E-02	536	3.55E-01	2.02E-02	435 ± 10	3.98E-04	1.99E-05	2.42E-04	1.34E-05	1.38 ± 0.04
60701	3.93E-01	3.18E-02	536	3.48E-01	1.97E-02	435 ± 10	4.16E-04	3.03E-05	2.27E-04	1.83E-05	1.38 ± 0.04
60701	4.01E-01	1.60E-02	536	3.51E-01	1.96E-02	435 ± 10	3.97E-04	2.56E-05	2.31E-04	1.52E-05	1.38 ± 0.04
40428	6.59E-01	5.02E-02	729	4.45E-01	2.44E-02	494 ± 11	4.27E-04	2.17E-05	2.72E-04	1.90E-05	1.58 ± 0.04
40428	6.33E-01	3.37E-02	729	4.49E-01	2.60E-02	494 ± 11	4.56E-04	3.04E-05	2.61E-04	1.79E-05	1.58 ± 0.04
40428	4.35E-01	3.16E-02	729	4.44E-01	2.49E-02	494 ± 11	4.65E-04	3.07E-05	5.04E-04	3.35E-05	1.58 ± 0.04
47963	1.16E+00	8.40E-02	1262	1.22E+00	8.14E-02	1356 ± 30	1.23E-03	7.29E-05	1.02E-03	6.11E-05	4.57 ± 0.11
47963	1.08E+00	6.33E-02	1262	1.06E+00	6.89E-02	1356 ± 30	1.27E-03	7.93E-05	7.58E-04	4.93E-05	4.57 ± 0.11
LoD (µg.g^{-1})	64			51			0.13		0.49		
13/07/2022											
47963	1.19E+00	9.10E-02	1262	1.05E+00	6.33E-02	1356 ± 30	1.23E-03	6.97E-05	1.29E-03	7.33E-05	4.57 ± 0.11
47963	1.08E+00	6.74E-02	1262	9.28E-01	4.60E-02	1356 ± 30	1.28E-03	6.83E-05	1.31E-03	6.86E-05	4.57 ± 0.11
60701	4.62E-01	3.60E-02	536	2.76E-01	1.51E-02	435 ± 10	4.38E-04	1.93E-05	3.86E-04	1.89E-05	1.38 ± 0.04
60701	6.51E-01	3.86E-02	536	3.15E-01	1.39E-02	435 ± 10	4.66E-04	2.57E-05	4.19E-04	2.46E-05	1.38 ± 0.04
60701	6.81E-01	3.70E-02	536	3.25E-01	1.76E-02	435 ± 10	4.44E-04	2.63E-05	3.99E-04	2.43E-05	1.38 ± 0.04
60701	5.07E-01	3.00E-02	536	3.35E-01	1.82E-02	435 ± 10	4.36E-04	2.56E-05	3.92E-04	2.36E-05	1.38 ± 0.04
25603	6.53E-01	3.07E-02	769	5.92E-01	2.47E-02	799 ± 17	7.92E-04	5.00E-05	7.74E-04	4.92E-05	2.64 ± 0.06
25603	5.45E-01	6.55E-02	769	5.87E-01	3.60E-02	799 ± 17	8.01E-04	4.35E-05	7.85E-04	4.36E-05	2.64 ± 0.06
25603	7.06E-01	4.88E-02	769	6.32E-01	3.78E-02	799 ± 17	7.45E-04	4.34E-05	7.65E-04	4.56E-05	2.64 ± 0.06
25603	6.37E-01	4.66E-02	769	6.16E-01	3.51E-02	799 ± 17	7.27E-04	3.04E-05	7.50E-04	3.21E-05	2.64 ± 0.06
VG2	2.29E-01	1.45E-02	334 ± 14	2.24E-01	1.20E-02	306 ± 13	4.20E-04	2.29E-05	4.71E-04	2.62E-05	NA
VG2	2.44E-01	9.64E-03	334 ± 14	2.39E-01	1.33E-02	306 ± 13	3.91E-04	2.08E-05	4.45E-04	2.45E-05	NA
VG2	2.07E-01	1.33E-02	334 ± 14	1.95E-01	9.46E-03	306 ± 13	3.74E-04	1.71E-05	3.82E-04	2.00E-05	NA
VG2	1.93E-01	9.13E-03	334 ± 14	2.23E-01	1.19E-02	306 ± 13	3.95E-04	2.03E-05	4.36E-04	2.42E-05	NA
LoD (µg.g^{-1})	113			49			0.19		0.07		

Table S-2 continued

	F			Cl			Br				
	$^{19}F/^{30}Si$	Error (σ)	F (µg.g^{-1})	$^{35}Cl/^{30}Si$	Error (σ)	Cl (µg.g^{-1})	$^{81}Br/^{30}SiO_3$	Error	$^{79}Br/^{30}SiO_3$	Error	Br (µg.g^{-1})
11/04/2019											
47963							3.70E-02	7.32E-04	3.52E-02	8.02E-04	4.57 ± 0.11
47963							3.65E-02	7.49E-04	3.52E-02	7.99E-04	4.57 ± 0.11
25603							2.31E-02	4.62E-04	2.03E-02	6.92E-04	2.64 ± 0.06
25603							2.30E-02	5.42E-04	2.05E-02	4.04E-04	2.64 ± 0.06
25603							2.32E-02	4.24E-04	1.92E-02	4.58E-04	2.64 ± 0.06
60701							1.60E-02	3.69E-04	1.24E-02	2.90E-04	1.38 ± 0.04
60701							1.59E-02	1.83E-04	1.25E-02	3.76E-04	1.38 ± 0.04
LoD (µg.g^{-1})							0.38		0.18		
12/09/2019											
47963	3.27E+00	1.77E-02	1262	1.99E+00	1.44E-02	1356 ± 30					
47963	3.26E+00	1.88E-02	1262	1.98E+00	1.60E-02	1356 ± 30					
47963	3.26E+00	2.11E-02	1262	1.98E+00	1.44E-02	1356 ± 30					
40428	1.89E+00	1.27E-02	729	7.01E-01	5.67E-03	494 ± 11					
40428	1.89E+00	1.14E-02	729	7.00E-01	4.21E-03	494 ± 11					
40428	1.89E+00	1.20E-02	729	6.97E-01	4.85E-03	494 ± 11					
VG2	6.34E-01	2.98E-03	334 ± 14	3.93E-01	2.30E-03	306 ± 13					
VG2	6.32E-01	3.72E-03	334 ± 14	4.00E-01	2.59E-03	306 ± 13					
VG2	6.46E-01	2.64E-03	334 ± 14	4.11E-01	2.97E-03	306 ± 13					
40428	1.89E+00	1.31E-02	729	6.99E-01	4.89E-03	494 ± 11					
40428	1.88E+00	1.27E-02	729	6.95E-01	4.61E-03	494 ± 11					
VG2	6.36E-01	4.66E-03	334 ± 14	4.12E-01	2.87E-03	306 ± 13					
VG2	6.27E-01	4.33E-03	334 ± 14	3.89E-01	2.16E-03	306 ± 13					
VG2	6.26E-01	4.47E-03	334 ± 14	4.01E-01	3.10E-03	306 ± 13					
47963	3.27E+00	1.96E-02	1262	2.01E+00	1.45E-02	1356 ± 30					
47963	3.26E+00	1.97E-02	1262	1.99E+00	1.72E-02	1356 ± 30					
47963	3.26E+00	1.74E-02	1262	2.00E+00	1.23E-02	1356 ± 30					
LoD (µg.g^{-1})	44			13							

Table S-3 Raw data and drift correction for calibration of $\delta^{37}Cl$. Reference values for B2-1 and B20D are +0.59 ‰ (± 0.33 ‰) and +0.95 ‰ (± 0.33 ‰), respectively (John *et al.*, 2010). MI – melt inclusion.

		$^{37}Cl/^{35}Cl$		^{35}Cl/Coeff		^{37}Cl/Coeff		yield	$\delta^{37}Cl$ raw		raw value		$\delta^{37}Cl$ corrected	
	(nA)	*H2/L1*	*1se*	*L1*	*1se*	*H2*	*1se*	*^{37}Cl cps/nA*	‰	*2se*	*bias to StH*	*IMF*	‰	*2se*
Reference material mount														
TiG	1.76	3.281E-01	2.15E-02	1.271E+05	9.489E-01	4.171E+04	9.44E-01	7.227E+04	26.64	0.43				
TiG	1.76	3.281E-01	2.16E-02	1.268E+05	8.773E-01	4.160E+04	8.81E-01	7.194E+04	26.59	0.43				
B2-1	1.76	3.265E-01	1.12E-02	1.014E+06	7.138E-01	3.311E+05	7.22E-01	5.768E+05	21.46	0.22	-6.24			
B2-1	1.75	3.267E-01	1.20E-02	9.984E+05	5.781E-01	3.262E+05	5.88E-01	5.697E+05	22.15	0.24	-5.56			
B20D	1.75	3.268E-01	1.04E-02	7.552E+05	5.053E-01	2.468E+05	5.13E-01	4.326E+05	22.52	0.21	-5.19	22.02		
B20D	1.74	3.269E-01	9.21E-03	7.081E+05	6.404E-01	2.314E+05	6.44E-01	4.066E+05	22.71	0.18	-4.99	22.21		
StH	1.73	3.283E-01	1.42E-02	2.943E+05	5.678E-01	9.664E+04	5.68E-01	1.699E+05	27.29	0.28				
StH	1.73	3.286E-01	1.45E-02	2.818E+05	5.442E-01	9.260E+04	5.45E-01	1.631E+05	28.13	0.29				
SC	1.72	2.803E-01	8.84E-01	4.960E+03	2.193E-01	1.391E+03	8.60E-01	2.880E+03	-122.86	17.67	blank			
Sample mount 1														
StH_mount1	1.69	3.285E-01	1.45E-02	2.806E+05	6.061E-01	9.217E+04	6.06E-01	1.656E+05	27.88	0.29	drift monitor			
CS5-3	1.70	3.269E-01	1.94E-02	1.575E+05	5.628E-01	5.148E+04	5.65E-01	9.269E+04	22.93	0.39			0.81	0.44
CS5-4	1.70	3.269E-01	2.05E-02	1.598E+05	5.016E-01	5.223E+04	5.13E-01	9.420E+04	22.79	0.41			0.67	0.46
bg_mount1	1.69	3.145E-01	2.94E-01	5.525E+03	1.610E+00	1.729E+03	1.31E+00	3.263E+03	-16.08	5.88	background			
CS5-5S	1.69	3.266E-01	2.27E-02	1.381E+05	4.428E-01	4.510E+04	4.50E-01	8.189E+04	22.04	0.45			-0.07	0.49
CS5-5L	1.68	3.270E-01	2.06E-02	1.388E+05	4.596E-01	4.538E+04	4.59E-01	8.258E+04	23.13	0.41			1.01	0.46
StH_mount1	1.67	3.285E-01	1.49E-02	2.847E+05	5.654E-01	9.353E+04	5.67E-01	1.704E+05	27.97	0.30	Drift monitor			
CS6-1	1.67	3.267E-01	2.13E-02	1.303E+05	4.266E-01	4.256E+04	4.31E-01	7.787E+04	22.16	0.43			0.04	0.47
Sample mount 2														
StH_mount2	1.65	3.285E-01	1.44E-02	2.835E+05	7.090E-01	9.315E+04	7.08E-01	1.723E+05	27.95	0.29	drift monitor			
PI-25_MI5	1.65	3.266E-01	2.12E-02	1.315E+05	5.735E-01	4.294E+04	5.78E-01	7.988E+04	21.99	0.42			-0.97	0.46
PI-25_MI7	1.64	3.273E-01	2.31E-02	1.453E+05	5.797E-01	4.758E+04	5.85E-01	8.853E+04	24.13	0.46			0.21	0.50
StH_mount2	1.63	3.292E-01	1.57E-02	2.799E+05	6.887E-01	9.213E+04	6.92E-01	1.712E+05	30.07	0.31	drift monitor			
bg_mount2	1.63	3.200E-01	2.88E-01	3.982E+03	9.707E-02	1.272E+03	3.36E-01	2.438E+03	1.43	5.77	background			
PI-25_MI9	1.63	3.275E-01	2.06E-02	1.387E+05	6.249E-01	4.542E+04	6.26E-01	8.517E+04	24.60	0.41			-0.09	0.45
PI-25_MI10	1.63	3.276E-01	2.02E-02	1.452E+05	7.090E-01	4.757E+04	7.15E-01	8.937E+04	24.91	0.40			0.03	0.45
PI-25_MI11	1.62	3.275E-01	2.10E-02	1.344E+05	6.070E-01	4.402E+04	6.08E-01	8.310E+04	24.70	0.42			-0.34	0.46
StH_mount2	1.62	3.294E-01	1.46E-02	2.767E+05	6.976E-01	9.111E+04	6.96E-01	1.713E+05	30.59	0.29	drift monitor			
PI-25_MI12	1.61	3.276E-01	2.66E-02	8.322E+04	3.447E-01	2.726E+04	3.53E-01	5.170E+04	25.01	0.53			-0.31	0.56
PI-25_MI15	1.61	3.277E-01	2.45E-02	9.846E+04	1.296E+00	3.227E+04	1.30E+00	6.133E+04	25.22	0.49			-0.22	0.52
PI-25_MI16	1.60	3.276E-01	1.66E-02	2.208E+05	7.701E-01	7.234E+04	7.75E-01	1.381E+05	25.18	0.33			-0.38	0.38
StH_mount2	1.60	3.296E-01	1.47E-02	2.744E+05	6.889E-01	9.043E+04	6.88E-01	1.718E+05	31.32	0.29	drift monitor			
PI-25_MI17	1.59	3.277E-01	2.10E-02	1.342E+05	6.107E-01	4.397E+04	6.17E-01	8.443E+04	25.39	0.42			-0.36	0.46
PI-25_MI20	1.59	3.279E-01	1.47E-02	2.721E+05	6.163E-01	8.921E+04	6.20E-01	1.716E+05	26.11	0.29			0.27	0.35
PI-25_MI19L	1.59	3.278E-01	2.09E-02	1.347E+05	6.475E-01	4.416E+04	6.52E-01	8.476E+04	25.64	0.42			-0.28	0.46
PI-25_MI19S	1.58	3.279E-01	2.11E-02	1.326E+05	6.141E-01	4.348E+04	6.20E-01	8.372E+04	25.92	0.42			-0.08	0.46
StH_mount2	1.58	3.299E-01	1.48E-02	2.701E+05	7.012E-01	8.910E+04	6.98E-01	1.713E+05	32.16	0.30	drift monitor			
StH_mount2	1.57	3.298E-01	1.48E-02	2.690E+05	6.788E-01	8.873E+04	6.78E-01	1.708E+05	32.03	0.30				
bg_mount2	1.57	3.396E-01	8.83E-02	7.039E+03	3.029E+00	2.394E+03	3.06E+00	4.486E+03	62.54	1.77	background			
StH_mount2	1.57	3.299E-01	1.49E-02	2.667E+05	6.903E-01	8.798E+04	6.89E-01	1.700E+05	32.16	0.30	drift monitor			
StH_mount2	1.56	3.299E-01	1.49E-02	2.655E+05	6.748E-01	8.760E+04	6.77E-01	1.702E+05	32.30	0.30	drift monitor			

Table S-4 Published values for key mixing reservoirs used to general fields in Figures 1 and 2.

K/Cl	average	1σ	Min.	Max.	reference
Subducted marine sediments (SMS)					
UCC	63	65			Rudnick and Gao (2014)
UCC	41				Wedepohl (1995)
Altered oceanic crust (AOC)					
Altered oceanic crust			0.3	2.0	Kendrick *et al.* (2013a)
Serpentinite					
Serpentinite	0.12	0.1	0.0	0.3	Kendrick *et al.* (2013b)
1000Br/Cl	**average**	**1σ**	**Min.**	**Max.**	**reference**
Subducted marine sediments (SMS)					
UCC	4.9	1.5	2	265	Han *et al.* (2023)
UCC	4.3				Rudnick and Gao (2014)
UCC	2.5				Wedepohl (1995)
sedimentary rock	5.7	5.4			Kendrick *et al.* (2017)
Altered oceanic crust (AOC)					
Layer 3 AOC	1.9	1.2			Kendrick (2018)
Altered oceanic crust				<2.5	Kendrick *et al.* (2014)
Altered oceanic crust			0	3.5	Kendrick (2019)
Altered oceanic crust	1.7	1.6			Chavrit *et al.* (2016)
Serpentinite					
Serpentinite	3.3	0.9			Kendrick (2018)
Serpentinite	5.5	1.9	2.7	10.4	Kendrick *et al.* (2013b)
Serpentinite	4.7	7.2			Chavrit *et al.* (2016)
$\delta^{37}Cl$	**average**	**1σ**	**Min.**	**Max.**	**reference**
Sediment and metasediment			-3.7	2.4	Bouvier *et al.* (2019)
Altered oceanic crust			-1.6	1.8	Bouvier *et al.* (2019)
Serpentinite			-2.7	2.4	Bouvier *et al.* (2019)
MORB			-1.04	0.37	Sharp *et al.* (2007)
$^{87}Sr/^{86}Sr$	**average**	**1σ**	**Min.**	**Max.**	**reference**
subducting sediments			0.7053	0.7080	Plank and Langmuir (1998)
Altered oceanic crust			0.7035	0.7075	Staudigel *et al.* (1995)
Serpentinite			0.7037	0.7095	Hattori and Guillot (2007)
DM			0.7020	0.7024	Zindler and Hart (1986)
$^{3}He/^{4}He$	**average**	**1σ**	**Min.**	**Max.**	**reference**
DM			11	7	Marty and Zimmermann (1999)

Table S-5 Partition coefficients used in source mantle calculation. Note, our bulk D_F and D_{Cl} differ from those in Joachim *et al.*, (2015) ($D_F = 0.08$ and $D_{Cl} = 0.03$), the reason for this are unclear, however their bulk partition coefficients can be reproduced using $D_F^{cpx}/D_F^{opx} = 5$ and $D_{Cl}^{cpx}/D_{Cl}^{opx} = 1.5$, rather than 1.5 and 5, respectively.

	X	D_F	D_{Cl}	D_{Br}	D_K
Olivine	0.62	0.028	0.029	0.029	0.0003
Orthopyroxene	0.24	0.066	0.027	0.027	0.0024
Clinopyroxene	0.12	0.098	0.136	0.136	0.0081
Bulk	0.98	0.045	0.041	0.041	0.0017

Table S-6 Composition of the N-PIP and E-PIP source calculated using the accumulated fractionation model based on samples PI-25 and CS-6, respectively. Compared to estimates for the composition of BSE, DM, lithospheric xenoliths and chondritic meteorites. Errors are 1 standard deviation.

	Method/Location	F (µg.g^{-1})	Cl (µg.g^{-1})	Br (µg.g^{-1})	1000Br/Cl
PIP source					
N-PIP source (PI-25, F=0.1)	Min-melt partitioning	19	9.2	0.104	11.3
E-PIP source (CS-6, F=0.25)	Min-melt partitioning	44	20	0.133	6.8
Depleted mantle					
Schilling *et al.* (1980)	Min-melt partitioning	65	7.3	0.02	2.74
Jambon *et al.* (1995)	Canonical ratio	-	~6	0.0075	1.25
Saal *et al.* (2002)	Canonical ratio	16 ± 3	1 ± 0.5	-	-
Salters and Stracke (2004)	Canonical ratio	11 ± 5	0.51 ± 0.09	-	-
Shimizu *et al.* (2016)	Canonical ratio	8.00	0.40	-	-
Joachim *et al.* (2015)	Min-melt partitioning	3-14	0.6-16	-	-
Kendrick *et al.* (2017)	Canonical ratio	12 ± 2	5 ± 2	0.013 ± 0.006	2.60
Guo and Korenaga (2021)	Log-log linear	54 ± 4.8	67 ± 26	0.049 ± 0.010	0.73
Bulk Silicate Earth					
McDonough and Sun (1995)	Canonical ratio	25	17	0.05	2.94
Palme and O'Neill (2014)	Mass balance + ratio	25 ± 10	30 ± 12	0.075 ± 0.038	2.50
Lyubetskaya and Korenaga (2007)	Canonical ratio	18 ±8	1.4 ± 0.5	0.0036 ± 0.0004	2.57
Kendrick *et al.* (2017)	Mass balance	17 ± 6	26 ± 8	0.076 ± 0.025	2.92
Guo and Korenaga (2021)	Log-log linear	57 ± 4.8	81 ± 24	0.091 ± 0.019	1.12
Intraplate lithospheric xenoliths					
Broadley *et al.* (2016)	West Antarctic				0.7-10
Kobayashi *et al.* (2019)	Eifel				0.5-4.5
Kobayashi *et al.* (2019)	Potrillo				0.1-4
Kobayashi *et al.* (2019)	San Carlos				3-7
CI Chondritic meteorites					
Wasson *et al.* (1997)	Compilation	64	680	3.6	5.29
Lodders and Fegley, 1998)	Compilation	60	717	3.34 ± 0.34	4.66
Palme and Zipfel (2022)	Orgueil	-	600 ± 68	2.68 ± 0.51	4.47
Palme and Zipfel (2022)	Ivuna	-	585	5.68	9.71
Palme and Zipfel (2022)	Alais	-	710	4.39	6.18
Palme and Zipfel (2022)	Tonk	-	510	9.01	17.7
CM Chondritic meteorites					
Wasson *et al.* (1997)	Compilation	38	160	2.6	16.3
Lodders and Fegley (1998)	Compilation	38	430	3	7.0
Reed and Allen (1966)	Mighei	-	350 ± 10	3.5 ± 1	10.0
Goles *et al.* (1967)	Mighei	-	430	3.9	9.1
Goles *et al.* (1967)	Mighei	-	510 ± 40	2.64 ± 0.03	5.2

Supplementary Figures

PI25-12 (mount 1)

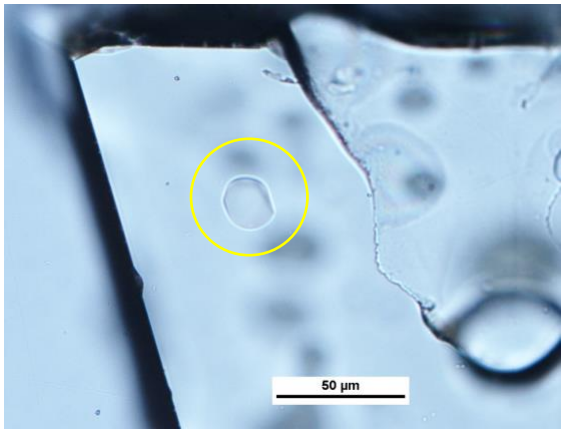

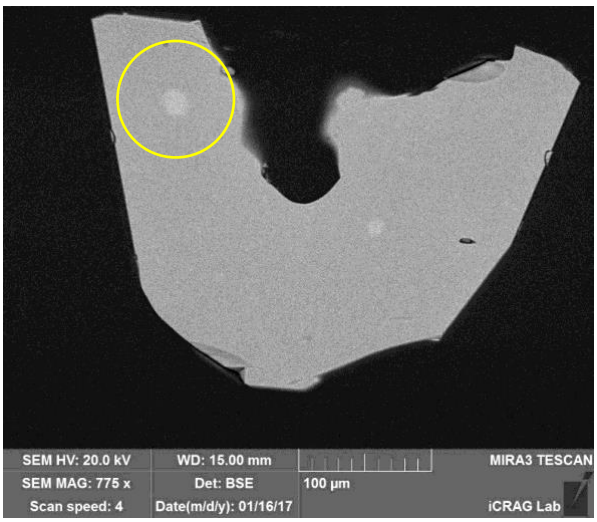

CS-5 3 (mount 3)

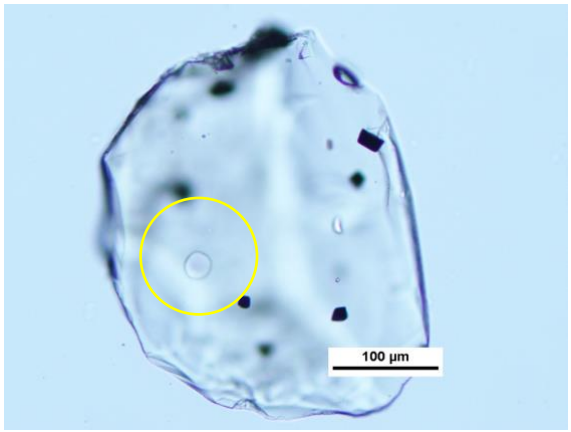

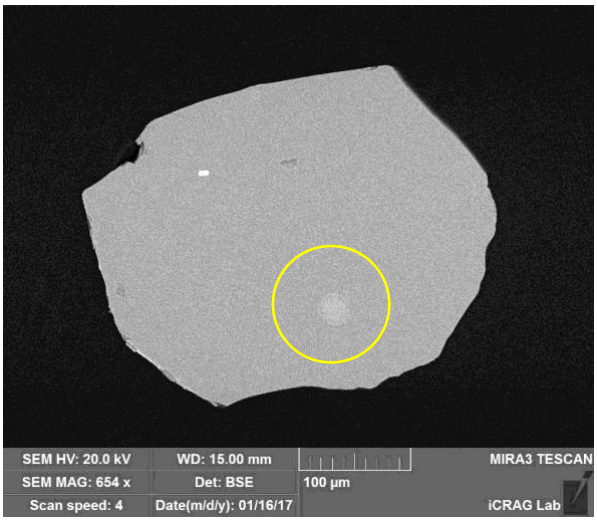

CS-6 1 (mount 3)

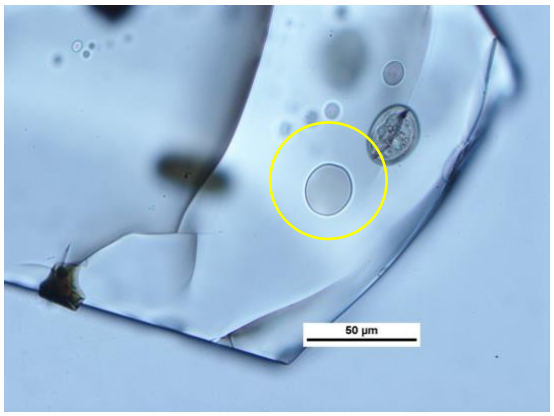

Figure S-1 Examples of the studied melt inclusions in transmitted light and Backscatter electron image.

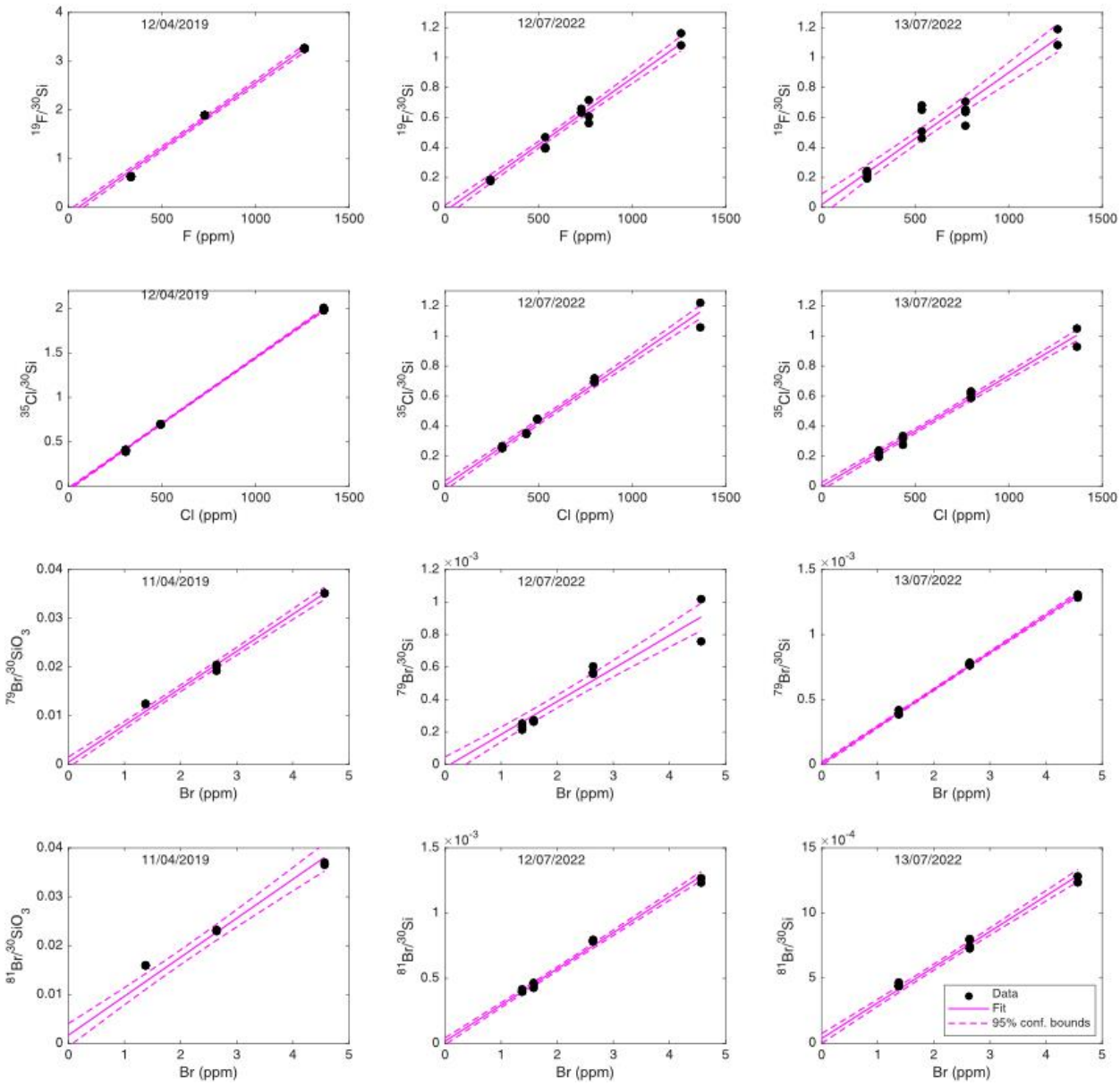

Figure S-2 Raw data for the calibration glass standards (in 2019: glasses VG-2, Macquarie 40428 and 47963; in 2022: glasses VG-2, Macquarie 25603, 40428, and 60701), the resulting calibration curves and their 95 % confidence intervals calculated by linear regression.

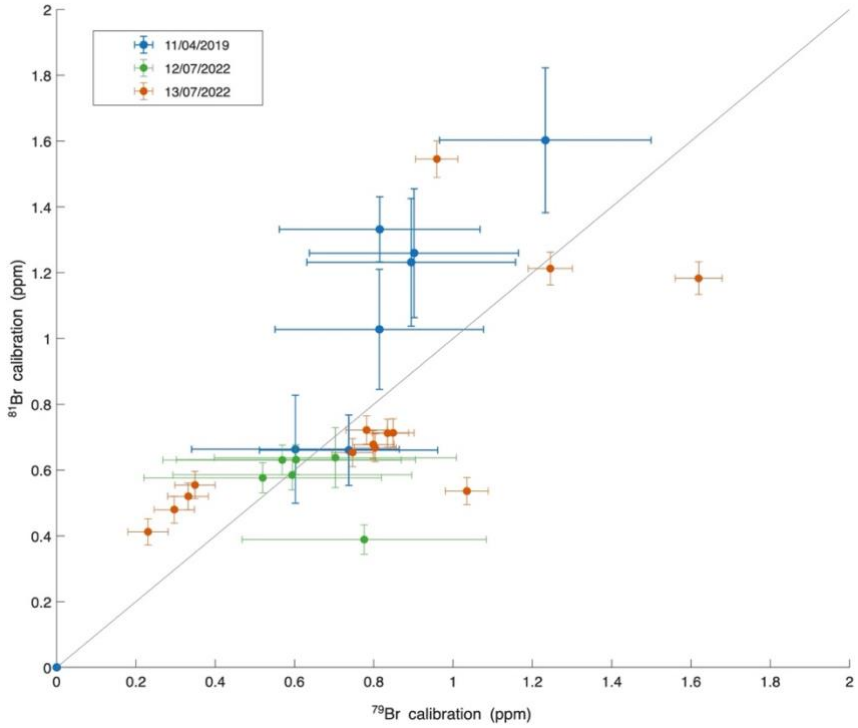

Figure S-3 Comparison between Br concentrations determined for unknowns (individual samples and quality control standards) using ^{81}Br and ^{79}Br, errors are propagated from the calibration curve.

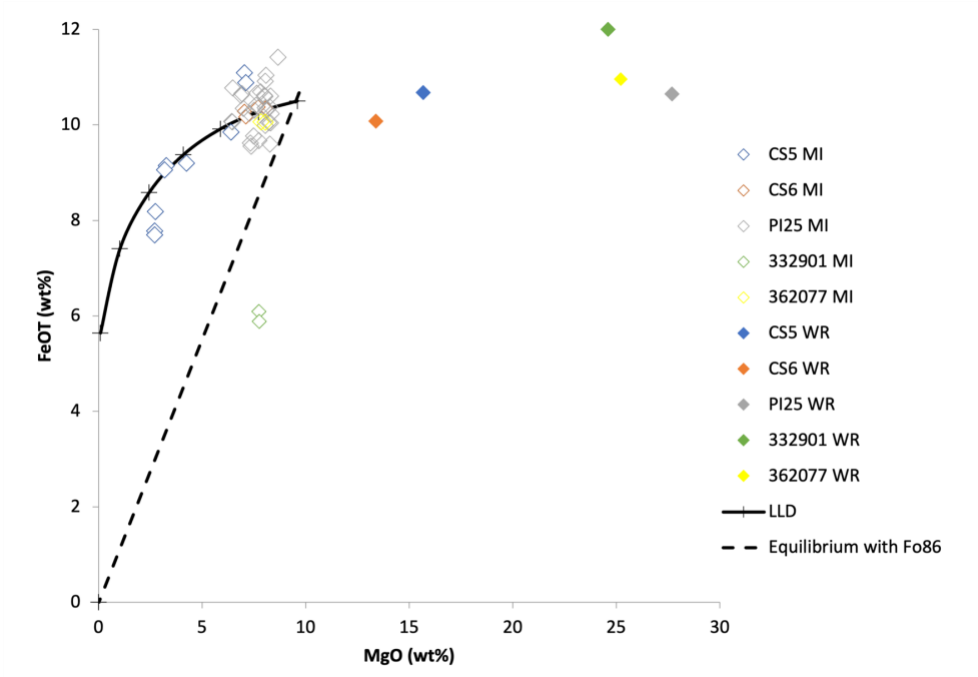

Figure S-4 Composition of PIP melt inclusions (this study) compared to the calculated liquid line of decent of melt DUR1 due to removal of olivine (+ markers show 5 % increments of olivine fractionation). Whole rock compositions are from Starkey *et al. (*2009). Also shown is the composition of melts in equilibrium with an olivine of a fixed composition of $Fo_{86.}$

Supplementary Information References

Bernstein, S., Hanghoj, K., Kelemen, P.B., Brooks, C.K. (2006) Ultra-depleted, shallow cratonic mantle beneath West Greenland: dunitic xenoliths from Ubekendt Ejland. *Contributions To Mineralogy and Petrology* 152, 335-347. https://doi.org/10.1007/s00410-006-0109-0

Bouvier, A.-S., Manzini, M., Rose-Koga, E.F., Nichols, A.R.L., Baumgartner, L.P. (2019) Tracing of Cl input into the sub-arc mantle through the combined analysis of B, O and Cl isotopes in melt inclusions. *Earth and Planetary Science Letters* 507, 30-39. https://doi.org/10.1016/j.epsl.2018.11.036

Broadley, M.W., Ballentine, C.J., Chavrit, D., Dallai, L., Burgess, R. (2016) Sedimentary halogens and noble gases within Western Antarctic xenoliths: Implications of extensive volatile recycling to the sub continental lithospheric mantle. *Geochimica et Cosmochimica Acta* 176, 139-156. https://doi.org/10.1016/j.gca.2015.12.013

Chavrit, D., Burgess, R., Sumino, H., Teagle, D.A.H., Droop, G., Shimizu, A., Ballentine, C.J. (2016) The contribution of hydrothermally altered ocean crust to the mantle halogen and noble gas cycles. *Geochimica et Cosmochimica Acta* 183, 106-124. https://doi.org/10.1016/j.gca.2016.03.014

Dalou, C., Koga, K.T., Le Voyer, M., Shimizu, N. (2014) Contrasting partition behavior of F and Cl during hydrous mantle melting: implications for Cl/F signature in arc magmas. *Progress in Earth and Planetary Science* 1, 26. https://doi.org/10.1186/s40645-014-0026-1

Dalou, C., Koga, K.T., Shimizu, N., Boulon, J., Devidal, J.L. (2012) Experimental determination of F and Cl partitioning between lherzolite and basaltic melt. *Contributions To Mineralogy and Petrology* 163, 591-609. https://doi.org/10.1007/s00410-011-0688-2

Dasgupta, R., Hirschmann, M.M., Smith, N.D. (2007) Partial Melting Experiments of Peridotite + CO_2 at 3 GPa and Genesis of Alkalic Ocean Island Basalts. *Journal of Petrology* 48, 2093-2124. https://doi.org/10.1093/petrology/egm053

Goles, G.G., Greenland, L.P., Jérome, D.Y. (1967) Abundances of chlorine, bromine and iodine in meteorites. *Geochimica et Cosmochimica Acta* 31, 1771-1787. https://doi.org/10.1016/0016-7037(67)90121-4

Guo, M., Korenaga, J. (2021) A halogen budget of the bulk silicate Earth points to a history of early halogen degassing followed by net regassing. *Proceedings of the National Academy of Sciences* 118, e2116083118-e2116083118. https://doi.org/10.1073/pnas.2116083118

Han, P.-Y., Rudnick, R.L., He, T., Marks, M.A.W., Wang, S.-J., Gaschnig, R.M., Hu, Z.-C. (2023) Halogen (F, Cl, Br, and I) concentrations of the upper continental crust through time as recorded in ancient glacial diamictite composites. *Geochimica et Cosmochimica Acta* 341, 28-45. https://doi.org/10.1016/j.gca.2022.11.012

Hattori, K.H., Guillot, S. (2007) Geochemical character of serpentinites associated with high- to ultrahigh-pressure metamorphic rocks in the Alps, Cuba, and the Himalayas: Recycling of elements in subduction zones. *Geochemistry, Geophysics, Geosystems* 8, Q09010. https://doi.org/10.1029/2007GC001594

Hauri, E.H., Gaetani, G.A., Green, T.H. (2006) Partitioning of water during melting of the Earth's upper mantle at H_2O-undersaturated conditions. *Earth and Planetary Science Letters* 248, 715-734. https://doi.org/10.1016/j.epsl.2006.06.014

Herzberg, C., O'Hara, M.J. (2002) Plume-associated ultramafic magmas of phanerozoic age. *Journal of Petrology* 43, 1857-1883. https://doi.org/10.1093/petrology/43.10.1857

Jackson, M.G., Shirey, S.B. (2011) Re–Os isotope systematics in Samoan shield lavas and the use of Os-isotopes in olivine phenocrysts to determine primary magmatic compositions. *Earth and Planetary Science Letters* 312, 91-101. https://doi.org/10.1016/j.epsl.2011.09.046

Jambon, A., Déruelle, B., Dreibus, G., Pineau, F. (1995) Chlorine and bromine abundance in MORB: the contrasting behaviour of the Mid-Atlantic Ridge and East Pacific Rise and implications for chlorine geodynamic cycle. *Chemical Geology* 126, 101-117. https://doi.org/10.1016/0009-2541(95)00112-4

Jarosewich, E., Nelen, J.A., Norberg, J. (1980) Reference samples for electron microprobe analysis. *Geostandards Newsletter* 4, 43-47. https://doi.org/10.1111/j.1751-908X.1980.tb00273.x

Joachim, B., Pawley, A., Lyon, I.C., Marquardt, K., Henkel, T., Clay, P.L., Ruzie, L., Burgess, R., Ballentine, C.J. (2015) Experimental partitioning of F and Cl between olivine, orthopyroxene and silicate melt at Earth's mantle conditions. *Chemical Geology* 416, 65-78. https://doi.org/10.1016/j.chemgeo.2015.08.012

Jochum, K.P., Stoll, B., Herwig, K., Willbold, M., Hofmann, A.W., *et al*. (2006) MPI-DING reference glasses for in situ microanalysis: New reference values for element concentrations and isotope ratios. *Geochemistry, Geophysics, Geosystems* 7, Q02008. https://doi.org/10.1029/2005GC001060

John, T., Layne, G.D., Haase, K.M., Barnes, J.D. (2010) Chlorine isotope evidence for crustal recycling into the Earth's mantle. *Earth and Planetary Science Letters* 298, 175-182. https://doi.org/10.1016/j.epsl.2010.07.039

Kendrick, M. (2018) Halogens in Seawater, Marine Sediments and the Altered Oceanic Lithosphere. In: Harlov, D.E., Aranovich, L. (Eds.) *The Role of Halogens in Terrestrial and Extraterrestrial Geochemical Processes*. Springer, 591-648. https://doi.org/10.1007/978-3-319-61667-4_9

Kendrick, M.A. (2019) Halogens in altered ocean crust from the East Pacific Rise (ODP/IODP Hole 1256D). *Geochimica et Cosmochimica Acta* 261, 93-112. https://doi.org/10.1016/j.gca.2019.06.044

Kendrick, M.A., Kamenetsky, V.S., Phillips, D., Honda, M. (2012) Halogen systematics (Cl, Br, I) in Mid-Ocean Ridge Basalts: A Macquarie Island case study. *Geochimica et Cosmochimica Acta* 81, 82-93. https://doi.org/10.1016/j.gca.2011.12.004

Kendrick, M.A., Arculus, R., Burnard, P., Honda, M. (2013a) Quantifying brine assimilation by submarine magmas: Examples from the Galapagos Spreading Centre and Lau Basin. *Geochimica et Cosmochimica Acta* 123, 150-165. https://doi.org/10.1016/j.gca.2013.09.012

Kendrick, M.A., Honda, M., Pettke, T., Scambelluri, M., Phillips, D., Giuliani, A. (2013b) Subduction zone fluxes of halogens and noble gases in seafloor and forearc serpentinites. *Earth and Planetary Science Letters* 365, 86-96. https://doi.org/10.1016/j.epsl.2013.01.006

Kendrick, M.A., Arculus, R.J., Danyushevsky, L.V., Kamenetsky, V.S., Woodhead, J.D., Honda, M. (2014) Subduction-related halogens (Cl, Br and I) and H_2O in magmatic glasses from Southwest Pacific Backarc Basins. *Earth and Planetary Science Letters* 400, 165-176. https://doi.org/10.1016/j.epsl.2014.05.021

Kendrick, M.A., Hémond, C., Kamenetsky, V.S., Danyushevsky, L., Devey, C.W., Rodemann, T., Jackson, M.G., Perfit, M.R. (2017) Seawater cycled throughout Earth's mantle in partially serpentinized lithosphere. *Nature Geoscience* 10, 222-228. https://doi.org/10.1038/ngeo2902

Kobayashi, M., Sumino, H., Burgess, R., Nakai, S.i., Iizuka, T., Nagao, J., Kagi, H., Nakamura, M., Takahashi, E., Kogiso, T., Ballentine, C.J. (2019) Halogen Heterogeneity in the Lithosphere and Evolution of Mantle Halogen Abundances Inferred From Intraplate Mantle Xenoliths. *Geochemistry Geophysics Geosystems* 20, 952-973. https://doi.org/10.1029/2018GC007903

Larsen, L.M., Pedersen, A.K. (2000) Processes in High-Mg, High-T Magmas: Evidence from Olivine, Chromite and Glass in Palaeogene Picrites from West Greenland. *Journal of Petrology* 41, 1071-1098. https://doi.org/10.1093/petrology/41.7.1071

Le Voyer, M., Rose-Koga, E.F., Shimizu, N., Grove, T.L., Schiano, P. (2010) Two Contrasting H_2O-rich Components in Primary Melt Inclusions from Mount Shasta. *Journal of Petrology* 51, 1571-1595. https://doi.org/10.1093/petrology/egq030

Lodders, K., Fegley, B. (1998) *The Planetary Scientist's Companion*. Oxford Academic. https://doi.org/10.1093/oso/9780195116946.001.0001

Lyubetskaya, T., Korenaga, J. (2007) Chemical composition of Earth's primitive mantle and its variance: 1. Method and results. *Journal of Geophysical Research: Solid Earth* 112, B03211. https://doi.org/10.1029/2005JB004223

Manzini, M., Bouvier, A.-S., Barnes, J.D., Bonifacie, M., Rose-Koga, E.F., Ulmer, P., Métrich, N., Bardoux, G., Williams, J., Layne, G.D., Straub, S., Baumgartner, L.P., John, T. (2017) SIMS chlorine isotope analyses in melt inclusions from arc settings. *Chemical Geology* 449, 112-122. https://doi.org/10.1016/j.chemgeo.2016.12.002

Marty, B., Zimmermann, L. (1999) Volatiles (He, C, N, Ar) in mid-ocean ridge basalts: assesment of shallow-level fractionation and characterization of source composition. *Geochimica et Cosmochimica Acta* 63, 3619-3633. https://doi.org/10.1016/S0016-7037(99)00169-6

McDonough, W.F. (1990) Constraints on the composition of the continental lithospheric mantle. *Earth and Planetary Science Letters* 101, 1-18. https://doi.org/10.1016/0012-821X(90)90119-I

McDonough, W.F., Sun, S.-s. (1995) The composition of the Earth. *Chemical Geology* 120, 223-253. https://doi.org/10.1016/0009-2541(94)00140-4

Palme, H., O'Neill, H.St.C. (2014) 3.1 - Cosmochemical Estimates of Mantle Composition. In: Holland, H.D., Turekian, K.K. (Eds.) *Treatise on Geochemistry*. Second Edition, Elsevier, Oxford, 1-39. https://doi.org/10.1016/B978-0-08-095975-7.00201-1

Palme, H., Zipfel, J. (2022) The composition of CI chondrites and their contents of chlorine and bromine: Results from instrumental neutron activation analysis. *Meteoritics and Planetary Science* 57, 317-333. https://doi.org/10.1111/maps.13720

Plank, T., Langmuir, C.H. (1998) The chemical composition of subducting sediment and its consequences for the crust and mantle. *Chemical Geology* 145, 325-394. https://doi.org/10.1111/maps.13720

Reed, G.W., Allen, R.O. (1966) Halogens in chondrites. *Geochimica et Cosmochimica Acta* 30, 779-800. https://doi.org/10.1016/0016-7037(66)90132-3

Roedder, P.L., Emslie, R.F. (1970) Olivine-Liquid Equilibrium. *Contributions To Mineralogy and Petrology* 29, 275-289. https://doi.org/10.1007/BF00371276

Rose-Koga, E.F., Koga, K.T., Devidal, J.-L., Shimizu, N., Le Voyer, M., Dalou, C., Döbeli, M. (2020) In-situ measurements of magmatic volatile elements, F, S, and Cl, by electron microprobe, secondary ion mass spectrometry, and heavy ion elastic recoil detection analysis. *American Mineralogist* 105, 616-626. https://doi.org/10.2138/am-2020-7221

Rose-Koga, E.F., Bouvier, A.S., Gaetani, G.A., Wallace, P.J., Allison, C.M. et al. (2021) Silicate melt inclusions in the new millennium: A review of recommended practices for preparation, analysis, and data presentation. *Chemical Geology* 570, 120145. https://doi.org/10.1016/j.chemgeo.2021.120145

Rudnick, R.L., Gao, S. (2014) 4.1 - Composition of the Continental Crust. In: Holland, H.D., Turekian, K.K. (Eds.) *Treatise on Geochemistry*. Second Edition, Elsevier, Oxford, 1-51. https://doi.org/10.1016/B978-0-08-095975-7.00301-6

Saal, A.E., Hauri, E.H., Langmuir, C.H., Perfit, M.R. (2002) Vapour undersaturation in primitive mid-ocean-ridge basalt and the volatile content of Earth's upper mantle. *Nature* 419, 451-455. https://doi.org/10.1038/nature01073

Salters, V.J.M., Stracke, A. (2004) Composition of the depleted mantle. *Geochemistry, Geophysics, Geosystems* 5, Q05B07. https://doi.org/10.1029/2003GC000597

Schiano, P. (2003) Primitive mantle magmas recorded as silicate melt inclusions in igneous minerals. *Earth-Science Reviews* 63, 121-144. https://doi.org/10.1016/S0012-8252(03)00034-5

Schilling, J.g., Bergeron, M.B., Evans, R., Smith, J.V., Bailey, D.K., Tarney, J., Dunham, K.C. (1980) Halogens in the mantle beneath the North Atlantic. *Philosophical Transactions of the Royal Society of London. Series A, Mathematical and Physical Sciences* 297, 147-178. https://doi.org/10.1098/rsta.1980.0208

Sharp, Z.D., Barnes, J.D., Brearley, a.J., Chaussidon, M., Fischer, T.P., Kamenetsky, V.S. (2007) Chlorine isotope homogeneity of the mantle, crust and carbonaceous chondrites. *Nature* 446, 1062-1065. https://doi.org/10.1038/nature05748

Shimizu, K., Saal, A.E., Myers, C.E., Nagle, A.N., Hauri, E.H., Forsyth, D.W., Kamenetsky, V.S., Niu, Y. (2016) Two-component mantle melting-mixing model for the generation of mid-ocean ridge basalts: Implications for the volatile content of the Pacific upper mantle. *Geochimica et Cosmochimica Acta* 176, 44-80. https://doi.org/10.1016/j.gca.2015.10.033

Sobolev, A.V. (1996) Melt Incusions in Minerals as a source of principlepetrological information. *Petrology* 4, 209-220.

Sobolev, A., Dmitriev, L., Barsukov, V., Nevsorov, V., Slutskii, A. (1980) The formation conditions of high magnesium olivines from the monomineral fraction of Luna-24 regolith. *Proc. 11th Lunar Sci. Conf.* 11, 105-116.

Starkey, N.A., Stuart, F.M., Ellam, R.M., Fitton, J.G., Basu, S., Larsen, L.M. (2009) Helium isotopes in early Iceland plume picrites: Constraints on the composition of high $^{3}He/^{4}He$ mantle. *Earth and Planetary Science Letters* 277, 91-100. https://doi.org/10.1016/j.epsl.2008.10.007

Starkey, N.A., Fitton, J.G., Stuart, F.M., Larsen, L.M. (2012) Melt inclusions in olivines from early Iceland plume picrites support high $^{3}He/^{4}He$ in both enriched and depleted mantle. *Chemical Geology* 306-307, 54-62. https://doi.org/10.1016/j.chemgeo.2012.02.022

Staudigel, H., Davies, G.R., Hart, S.R., Marchant, K.M., Smith, B.M. (1995) Large scale isotopic Sr, Nd and O isotopic anatomy of altered oceanic crust: DSDP/ODP sites 417/418. *Earth and Planetary Science Letters* 130, 169-185. https://doi.org/10.1016/0012-821X(94)00263-X

Stephan, T., Jessberger, E.K., Klöck, W., Rulle, H., Zehnpfenning, J. (1994) TOF-SIMS analysis of interplanetary dust. *Earth and Planetary Science Letters* 128, 453-467. https://doi.org/10.1016/0012-821X(94)90162-7

Straub, S.M., Layne, G.D. (2003) The systematics of chlorine, fluorine, and water in Izu arc front volcanic rocks: Implications for volatile recycling in subduction zones. *Geochimica et Cosmochimica Acta* 67, 4179-4203. https://doi.org/10.1016/S0016-7037(03)00307-7

Stuart, F.M., Lass-Evans, S., Fitton, J.G., Ellam, R.M. (2003) High $^{3}He/^{4}He$ ratios in picritic basalts from Baffin Island and the role of a mixed reservoir in mantle plumes. *Nature* 424, 57-59. https://doi.org/10.1038/nature01711

Wasson, J.T., Kallemeyn, G.W., Runcorn, S.K., Turner, G., Woolfson, M.M. (1997) Compositions of chondrites. *Philosophical Transactions of the Royal Society of London. Series A, Mathematical and Physical Sciences* 325, 535-544. https://doi.org/10.1098/rsta.1988.0066

Wedepohl, K.H. (1995) The composition of the continental crust. *Geochimica et Cosmochimica Acta* 59, 1217-1232. https://doi.org/10.1016/0016-7037(95)00038-2

Zindler, A., Hart, S.R. (1986) Chemical Geodynamics. *Annual Reviews of Earth and Planetary sciences* 14, 493-571. https://doi.org/10.1146/annurev.ea.14.050186.002425